SCIENTIFIC REPORTS

Accidental degeneracy of double Dirac cones in a phononic crystal

Ze-Guo Chen[1], Xu Ni[1], Ying Wu[2], Cheng He[1], Xiao-Chen Sun[1], Li-Yang Zheng[1], Ming-Hui Lu[1]
& Yan-Feng Chen[1]

[1]National Laboratory of Solid State Microstructures & Department of Materials Science and Engineering, Nanjing University,
Nanjing 210093, People's Republic of China, [2]Division of Mathematical and Computer Sciences and Engineering, King Abdullah
University of Science and Technology (KAUST), Thuwal 23955-6900, Saudi Arabia.

Artificial honeycomb lattices with Dirac cone dispersion provide a macroscopic platform to study the massless Dirac quasiparticles and their novel geometric phases. In this paper, a quadruple-degenerate state is achieved at the center of the Brillouin zone in a two-dimensional honeycomb lattice phononic crystal, which is a result of accidental degeneracy of two double-degenerate states. In the vicinity of the quadruple-degenerate state, the dispersion relation is linear. Such quadruple degeneracy is analyzed by rigorous representation theory of groups. Using $\vec{k} \cdot \vec{p}$ method, a reduced Hamiltonian is obtained to describe the linear Dirac dispersion relations of this quadruple-degenerate state, which is well consistent with the simulation results. Near such accidental degeneracy, we observe some unique properties in wave propagating, such as defect-insensitive propagating character and the Talbot effect.

Many unique phenomena in graphene such as quantum Hall effect, *Zitterbewegung*, Klein paradox and pseudo-diffusion, are attributed to the unique dispersion relation of massless quasiparticles solved by Dirac equation[1–5]. The eigen-energy E is linearly proportional to the wave vector k at the six corners of the hexagonal boundary of the Brillouin zone (BZ). The upper and lower bands near the K point act as two cones touching at one degenerate point, which is the so-called Dirac point and such conical dispersion is called a Dirac cone. Compared to Dirac cone dispersion at the corner of the BZ in graphene or photonics and phononics[6–10], the recent observation of Dirac cones at the center of the BZ in photonic and phonic crystals (PC) has also attracted much attention. Under certain circumstances, those Dirac cones can be mapped into a zero-refractive-index material, whose parameters (e.g. permittivity and permeability in electromagnetics, effective mass density and reciprocal of bulk modulus in acoustics) are both vanishing[11–15]. It provides a new method to achieve zero-index materials with simple photonic and phononic crystals so that many interesting properties such as wave shaping and cloaking are easily demonstrated[12,13,16,17].

Linear dispersion is a key feature of a Dirac cone. However, the linear dispersion at a finite frequency is in general forbidden at the center of the BZ, because of time-reversal symmetry[18,19]. The previously mentioned linear dispersion relations at the center of the BZ in classical wave systems are achieved by *accidental degeneracy*. In 2D photonic and phononic crystals with C_{4v} symmetry[11–13], it has been demonstrated that the accidental degeneracy of a monopolar state (or a quadrupolar state) and a double-degenerate dipolar state can lead to three-folded degeneracy showing linear dispersion in the vicinity of the Γ point. In addition to the linear bands, there is a flat band intersecting with them at the Dirac point. This is a major difference from the Dirac cones observed in graphene system, in which only two linear bands touch at the Dirac point. From a perturbation theory, it has been demonstrated that the Dirac cone induced by the triple-degenerated states at the center of the BZ is not a truly a Dirac cone because the reduced Hamiltonian cannot be casted into a Dirac equation (corresponding to three states) and the Berry phase equals to zero. Therefore, to be more precise, it is called a Dirac-like cone[20]. Recently, the double Dirac cone degeneracy at the BZ center has been predicted in triangular-lattice metamaterials with C_{6v} symmetry[21]. However, to the best of our knowledge, such quadruple-degenerate linear dispersion is still not realized in ordinary dielectric photonic crystals or phononic crystals, and furthermore, the underlying physics, such as the reduced Hamiltonian and the Berry phase, still remains unexplored. Meanwhile, such quadruple-degenerate Dirac-like cone states may also be expected to have rich physics that give rise to unique wave propagating properties to be explored.

In this paper, we demonstrate that a quadruple-degenerate state can be created at the BZ center by accidental degeneracy of E_1 and E_2 modes in a two-dimensional phononic crystal with honeycomb lattice. In the vicinity of
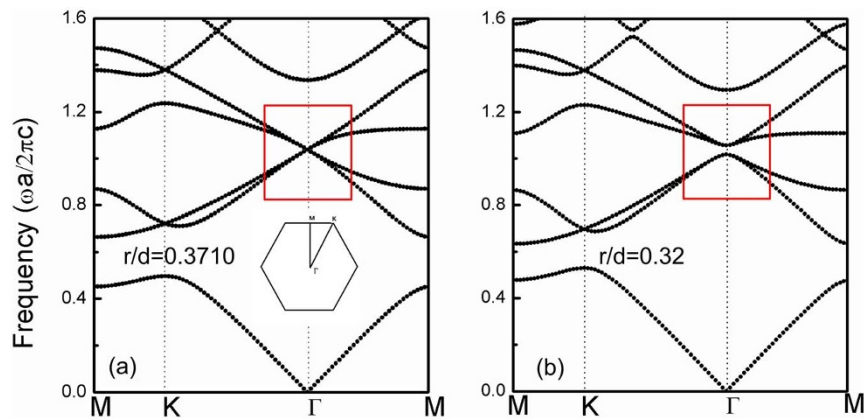
Figure 1 | (a) Band structures of a 2D honeycomb lattice PC consisting of iron cylinders (radius $r = 0.3710d$) in water. Four linear bands intersect at one point of $\omega_0 = 1.0378 \cdot (2\pi c/a)$ in red rectangle region. (b) Band structure with cylindrical radius $r = 0.32$ d, the degeneracy is lift.
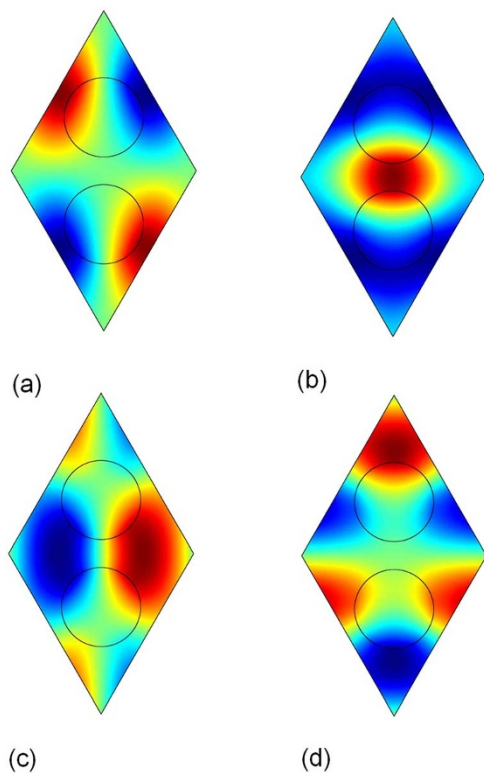
the quadruple-degenerate state, the dispersion relation is linear, with four cones touching at their vertices. Different from the Dirac-like cone induced by triple-degenerate state, there is no flat branch. We perform a symmetry analysis to prove the linearity of the dispersion relation and employ a $\vec{k}\cdot\vec{p}$ method to accurately predict the slope of the linear dispersion. The results of the $\vec{k}\cdot\vec{p}$ method also unambiguously reveal that the reduced Hamiltonian can be mapped into a 4×4 massless Dirac equation but the Berry phase cancels out due to the absence of imaginary part in Dirac equation. Moreover, based on such quadruple Dirac-like degeneracy, a novel defect-insensitive propagating phenomenon and the Talbot effects in such phononic crystals are well described with the acoustic field distribution obtained by the finite element simulation.

Figure 2 | (a–d) Pressure field distributions of four degenerate Bloch states at Γ point as indicated in Fig. 1(a) corresponding to ψ_1, ψ_2, ψ_3 and ψ_4 from low band to high, respectively. Dark red and dark blue colors denote the positive and negative values.

Results

The 2D PC considered here is composed of a honeycomb array of iron cylinders embedded in water ($\rho_1 = 1000$ kg/m^3, $c_1 = 1490$ m/s and $\rho_2 = 7670$ kg/m^3, $c_2 = 6010$ m/s, where ρ and c denote mass density and velocity of sound and subscripts 1 and 2 correspond to water and iron, respectively). The distance between two cylinders in one unit cell is $d = 1$ m, the lattice constant is $a = \sqrt{3}m$ and the radius of the cylinder is $r = 0.3710$ m. Because of the large difference in sound velocities between iron and water, the shear modes inside the iron cylinders can be ignored[22,23].

Figure 1(a) shows the band structure of the PC. It exhibits four bands touching linearly at one point at the frequency $\omega_0 = 892.77$ Hz at the center of the BZ, forming four cones. Such double Dirac cones are resulted from accidental degeneracy, which is clearly demonstrated in Fig. 1(b) when the radii of the cylinders are changed to $r = 0.32$ m. The quadruple-degenerate state shown in Fig. 1(a) is splitted into two double-degenerate states and the linear dispersion disappears. Since we are interested in the linear dispersion near the Γ point, we choose a region denoted by the red rectangle shown in Fig. 1 as our focus. Different from the triply degenerate case[11], there is no flat branch intersection in our model. Four cones are formed by the linear branches and touches at one point at the frequency of $\omega_0 = 892.77$ Hz with tolerance of 10^{-6}. These four eigen degenerate states are shown in Figs. 2(a–d).

Firstly, we employ the group theory to analyze the band structure. By examining the symmetry of the eigenstates at the degenerate point, one can check whether the dispersion near that point is linear or not[24]. According to the group theory, the Bloch states at Γ point with C_{6v} symmetry can be described as the basis of the irreducible representation based on the symmetry properties of the states[25]. The four eigen states match well with the four Bloch basis functions as shown in Table 1. The two double-degenerated states which result in the quadruple-degenerate state when they meet together correspond to E_1 and E_2 irreducible representations respectively. When any symmetry operation of C_{6v} is performed, the eigenfunction of E_1 state transforms like x and y, and E_2 state transforms like $2xy$ and

Table 1 | Four states at Γ point corresponding to four Bloch bases classified under different symmetry operation of C_{6v} group. ψ_1–ψ_4 correspond to field distributions in Figs. 2(a–d), respectively

C_{6v}	Basis	σ_x	σ_y
E_1	ψ_3, x	-1	1
	ψ_4, y	1	-1
E_2	ψ_1, xy	-1	-1
	ψ_2, $x^2 - y^2$	1	1

$x^2 - y^2$. The wave functions near the degenerated point can be expressed as linear combinations of the degenerate states. (These linear combination wave functions are also adopted in $\vec{k}\cdot\vec{p}$ method in the next section.) It should be noted that even under the same operation, the transformation of the Bloch state constructed of E_1 is different from that of E_2. Under the symmetry operations of σ_x and σ_y, E_1 and E_2 representation can further be classified into four states. Consequently, the double Dirac cone induced by the accidental degeneracy shown in Fig. 1(a) is supported by the group theory analysis[21]. The states near the Dirac point are linear combinations of the Bloch states with parity of σ_x or σ_y, and the wave equation should possess the same parity. Moreover, considering the compatibility relation along ΓK and ΓM directons, $E_1 = A + B$, $E_2 = A + B$, where A is full symmetry representation which indicates the existence of isotropic linear dispersion[25].

Then, we resort to the well-known $\vec{k}\cdot\vec{p}$ method in electronics to analyze our phononic model[20]. We can rewrite the Bloch functions near $\vec{k}_0$ as linear combinations of four $\vec{k}_0$ states. Substituting such function into wave equation with periodic boundary conditions, we can get[20]

$$\det\left|H - \frac{\omega_{n\vec{k}}^2 - \omega_{j0}^2}{c_1^2}I\right| = 0,\tag{1}$$

where n denotes the band index, $\vec{k}$ is the Bloch wave vector, and H is the reduced Hamiltonian matrix with element $H_{ij} = i\vec{k}\cdot\vec{L}_{ij}$, i and j are subscripts of matrix elements. Here, $\vec{L}_{ij}$ is a real vector in x-y plane. The x component of $\vec{L}_{ij}$ can be numerically calculated from the Bloch states as,

$$L_{ij}(x) = \frac{(2\pi)^2}{\Omega}\left(\int_{unitcell}\psi_{i\vec{k}_0}^*(\vec{r})\times\frac{2\frac{\partial\psi_{j\vec{k}_0}^*(\vec{r})}{\partial x}}{\rho_r(\vec{r})}d\vec{r} + \oint\psi_{i\vec{k}_0}^*(\vec{r}_0)\times\frac{\rho_r-1}{\rho_r}\times\cos(\theta)\times\psi_{j\vec{k}_0}^*(\vec{r}_0)d\vec{r}_0\right),\tag{2}$$

where $\rho_r(\vec{r}) = \rho(\vec{r})/\rho_1$, θ is the integration variable. The y component of $\vec{L}_{ij}$ can be calculated using the same process. In Eq. (2), only eight vectors are nonzero. Considering the anti-symmetrical property: $\vec{L}_{ij} = -\vec{L}_{ji}$, only four vectors are independent, and the relationships of these four vectors can be described as [shown in Fig. 3(a)]

$$\vec{L}_{13} = -\vec{L}_{24},\ \vec{L}_{23} = \vec{L}_{14},\ \vec{L}_{13}\cdot\vec{L}_{23} = 0$$

$$\vec{L}_{13} = (-0.03768, 4.0005),\ \vec{L}_{14} = (4.0009, 0.03768)\tag{3}$$

$$\vec{L}_{23} = (4.0011, 0.03766),\ \vec{L}_{24} = (0.03766, -4.0014).$$

Thus, the reduced Hamiltonian H can be casted into:

$$H = \begin{vmatrix} 0 & 0 & i\vec{k}\cdot\vec{L}_{13} & i\vec{k}\cdot\vec{L}_{14} \\ 0 & 0 & i\vec{k}\cdot\vec{L}_{23} & i\vec{k}\cdot\vec{L}_{24} \\ -i\vec{k}\cdot\vec{L}_{13} & -i\vec{k}\cdot\vec{L}_{23} & 0 & 0 \\ -i\vec{k}\cdot\vec{L}_{14} & -i\vec{k}\cdot\vec{L}_{24} & 0 & 0 \end{vmatrix}.\tag{4}$$

For the Bloch state at $\vec{k}$ in the vicinity of the Γ point, the angle between the Bloch wave vector and $\vec{L}_{13}$ is θ, by using Eq. (1), we can get dispersion relations of two Dirac cones

$$\frac{\Delta\omega}{\Delta k} = \pm\frac{|\vec{L}|c_1^2}{2\omega_0},\tag{5}$$

$\Delta\omega = \omega - \omega_0$ and $\Delta k = k - k_0$. Eq. (5) is linear in Δk and is independent of θ indicating the isotropy of the dispersion relation, which could be confirmed by the numerical simulations shown by solid dots in Fig. 3(b), and the isotropic equi-frequency contours (EFCs) shown in Figs. 4(b1) and (b2) result from the coupling of the degenerate Bloch state[21], which match well with the prediction of the group theory.

Knowing the length of $\vec{L}_{13}$, we can analytically calculate the dispersion relations from Eq. (5) as the red lines shown in Fig. 3(b), which overlaps with the solid dots well in the BZ center. It should be noted that although Eq. (5) exhibits only two roots, there should be four solutions to Eq (1), which means each root represented in Eq. (5) corresponds to two identical (degenerate) solutions. This is an important result, as it indicates that rather than having Dirac cones with different linear slopes, the Dirac cones produced here by the quadruple-degenerate state have identical slopes. This theoretical prediction is consistent with the simulated band structure [shown in Fig. 3(b)]. The equivalent frequency contours (EFCs) of these four bands are plotted in Fig. 4. Near the Dirac point, there is only one circle in the EFCs, verifying the isotropic property [Figs. 4(b1) and 4(b2) are identical]. Away from the Dirac point, apparently seen from Figs. 4(a) and 4(c), the EFCs for different bands are different and their hexagonal shapes indicate the anisotropy of the dispersion.

The linear dispersion at the Γ point described above is very similar to the Dirac point at the BZ corner studied earlier[5]. It has been reported that in a phononic crystal the Dirac point at the corner of the BZ carries nonzero Berry phase[26], while the Dirac-like point with triple degeneracy at Γ point carries zero Berry phase[20]. Now, we have achieved double Dirac cone at the Γ point by quadruple-degenerate state, does it carry zero or nonzero Berry phase? To answer this question, we perform the following analysis.
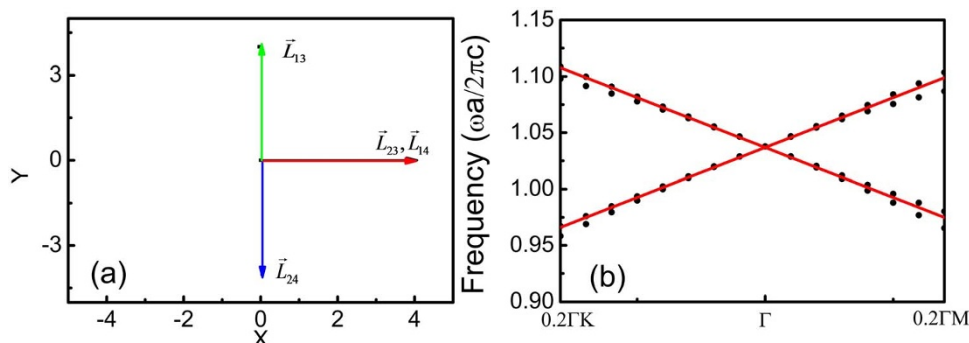
Figure 3 | (a) The relations of four vectors [seen in Eq.3] in real space calculated by field distribution in Fig. 2. These four real vectors have the same length. (b) Dirac dispersion relation. Dots and solid lines represent the simulation results and $\vec{k}\cdot\vec{p}$ method results, respectively.
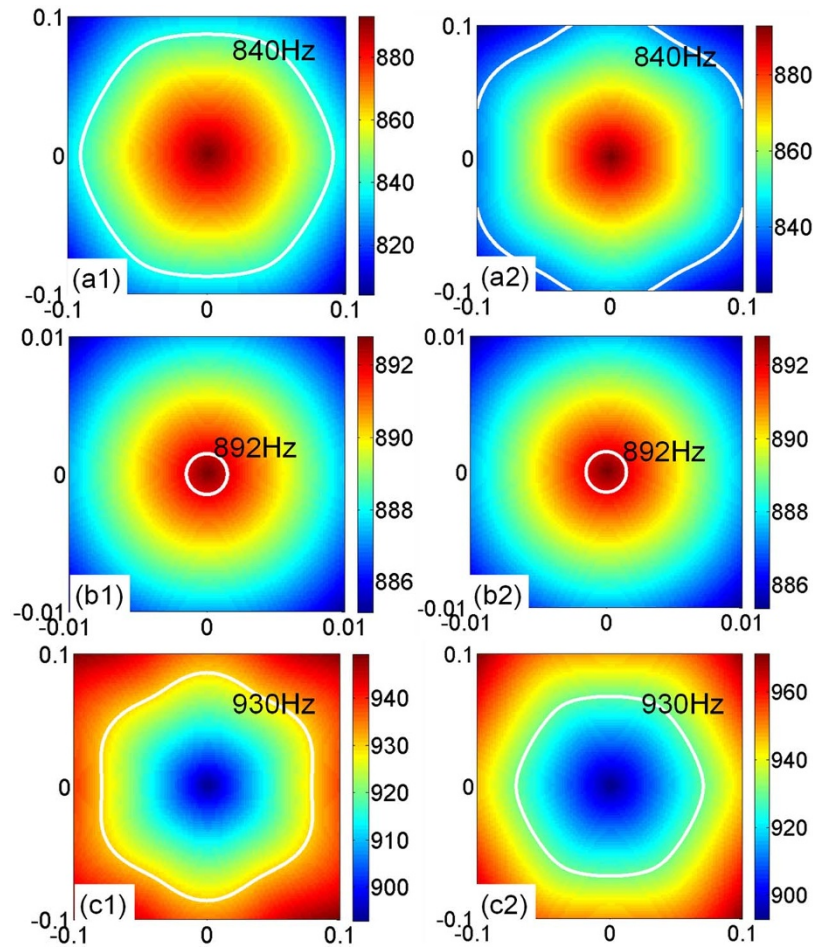
Figure 4 | Two EFCs corresponding to different bands at the frequencies of 840 *Hz*, 892 *Hz*, 930 *Hz*. (a1) and (a2) are EFCs of 840 *Hz*. (b1) and (b2) are EFCs of 892 *Hz* near Dirac points. (c1) and (c2) are EFCs of 930 *Hz*.

The eigenfunction of the H near $\vec{k}_0$ is

$$\varphi_1(\vec{k}) = \frac{1}{\sqrt{2}} \begin{pmatrix} i\sin\theta \\ -i\cos\theta \\ 0 \\ 1 \end{pmatrix} e^{i\vec{k}\cdot\vec{r}} \quad \varphi_2(\vec{k}) = \frac{1}{\sqrt{2}} \begin{pmatrix} i\cos\theta \\ i\sin\theta \\ 1 \\ 0 \end{pmatrix} e^{i\vec{k}\cdot\vec{r}}$$

$$\varphi_3(\vec{k}) = \frac{1}{\sqrt{2}} \begin{pmatrix} -i\sin\theta \\ i\cos\theta \\ 0 \\ 1 \end{pmatrix} e^{i\vec{k}\cdot\vec{r}} \quad \varphi_4(\vec{k}) = \frac{1}{\sqrt{2}} \begin{pmatrix} -i\cos\theta \\ -i\sin\theta \\ 1 \\ 0 \end{pmatrix} e^{i\vec{k}\cdot\vec{r}}, \tag{6}$$

We can calculate the Berry phase as,

$$\Gamma_i = i\cdot \oint \left\langle \varphi_i(\vec{k}) \middle| \nabla_{\vec{k}} \middle| \varphi_i(\vec{k}) \right\rangle \cdot d\vec{k}. \tag{7}$$

Taking $\varphi_1(\vec{k})$ as an example, we can write $\sin\theta = \dfrac{uk_x - vk_y}{k}$, $\cos\theta = \dfrac{vk_x + uk_y}{k}$, where $u^2 + v^2 = 1$. Substituting $\varphi_1(\vec{k})$ into Eq. (7), we find

$$\Gamma_i = i\cdot \oint \left\langle \varphi_i(\vec{k}) \middle| \nabla_{\vec{k}} \middle| \varphi_i(\vec{k}) \right\rangle \cdot d\vec{k}$$

$$= \frac{i}{2} \oint \left[-\frac{i}{k}(uk_x - vk_y), \frac{i}{k}(vk_x + uk_y), 0, 1 \right]$$

$$\times \left\{ \begin{bmatrix} \frac{i}{k}(u\vec{x} - v\vec{y}) \\ \frac{-i}{k}(v\vec{x} + u\vec{y}) \\ 0 \\ 0 \end{bmatrix} + \begin{bmatrix} \frac{i}{k}(uk_x - vk_y) \\ \frac{-i}{k}(vk_x + uk_y) \\ 0 \\ 1 \end{bmatrix} i\vec{r} \right\} \cdot d\vec{k} \tag{8}$$

$$= \frac{i}{2} \oint \left[\frac{1}{k^2}(k_x dk_x + k_y dk_y) \right] + \frac{i}{2} \oint 2i\vec{r}d\vec{k}$$

$$= 0,$$

The same result can be obtained if we use any $\varphi_i(\vec{k})$ in Eq. (7), which means the Berry phase for our system at Γ point is zero.

In other words, the H of our system can be written as

$$H = -\vec{L}_{14}\cdot\vec{k}\sigma_y \otimes \tau_x - \vec{L}_{13}\cdot\vec{k}\sigma_y \otimes \tau_z. \tag{9}$$

σ_y, τ_x, τ_z are all Pauli matrices and two Kronecker product matrices satisfy the anti-commutation relations. Although Eq. (9) is in the form of a massless Dirac equation, $\vec{L}_{14}\cdot\vec{k}$ and $\vec{L}_{13}\cdot\vec{k}$ contain no imaginary parts indicating the zero Berry phase, which is different from the Dirac cone at the corner of the BZ.
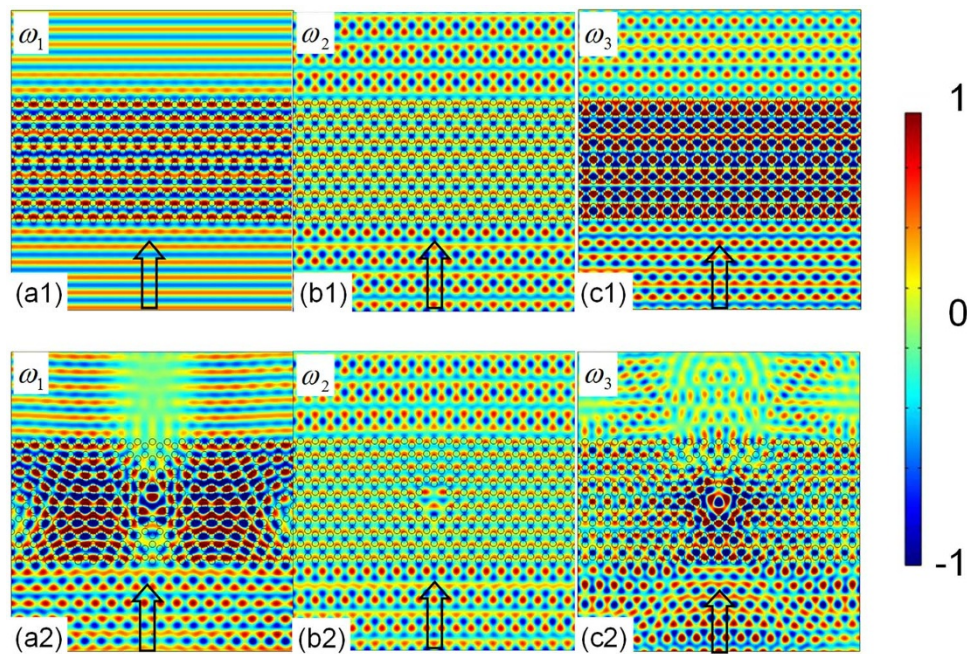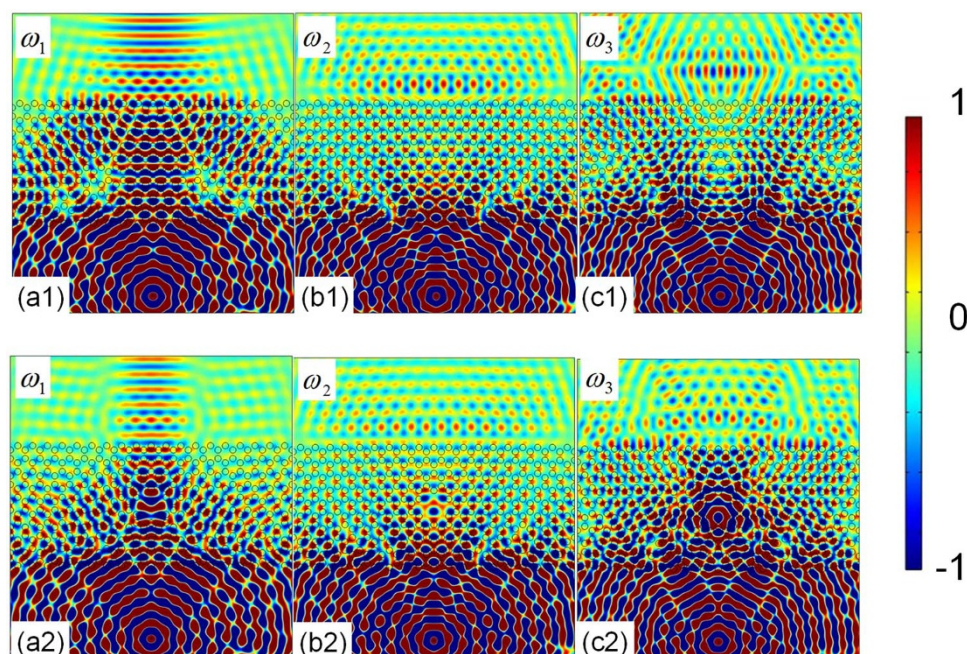
Figure 5 | Transmission patterns with plane incidence source. Operation frequencies are set at (a) ω_1, (b) ω_2 (c) ω_3. The suffix 1 or 2 represents the case of PC without or with defect, respectively. (b1) and (c1) exhibit the Talbot effect. (b2) shows the defect-immune property.

Finally, we analyze the wave propagating properties in our system near our concerned frequency. Figure 5 shows the numerical simulations of the wave propagating properties in the PC. In panels a1 and a2, we set the operating frequency to be $\omega_1 = 0.9409\omega_0$ below the frequency of Dirac point, $\omega_2 = 0.9991\omega_0$ is used in panels b1 and b2 near ω_0, $\omega_3 = 1.0417\omega_0$ is used in panels c1 and c2. The incident wave is along ΓM direction. Figure 5(a1) shows that the outgoing wave preserves the plane wave front, while Fig. 5(b1) shows the Talbot effect[27]. The Talbot effect is a near-field diffraction effect which was first observed in the year of 1836[28], and in this effect a plane wave transmits through a grating or other periodic structures with the resulting wave fronts propagating in such a way that replicates the structure. According to the field distribution shown in Fig. 5(b1), 5(c1), the wave fronts out of the PC share almost the same shape, while only Fig. 5(a1) returns into a plane wave after propagating about 2.3 wavelengths distance. Noted that the widely used effective medium theory is no longer applicable at such high frequency, and we cannot expect a plane wave at frequency ω_2 in the PC with C_{6v} symmetry. Here, ω_1 is a threshold frequency to reconstruct the plane wave. For a slight blue shift of frequency ω_1, we can find Talbot effect in our system as shown in Fig. 5(c1).

The defect insensitivity of the Talbot effect in our PC is also investigated and the results are shown in Figs. 5(a2), 5(b2) and 5(c2). Comparing with Dirac point at K point or Dirac-like point at Γ point

Figure 6 | Transmission patterns with cylindrical incidence source. Operation frequencies are set at (a) ω_1, (b) ω_2, (c) ω_3. The suffix 1 or 2 represents the case of PC without or with defect. (b1) and (c1) exhibit the Talbot effect. (b2) shows the defect-immune property.
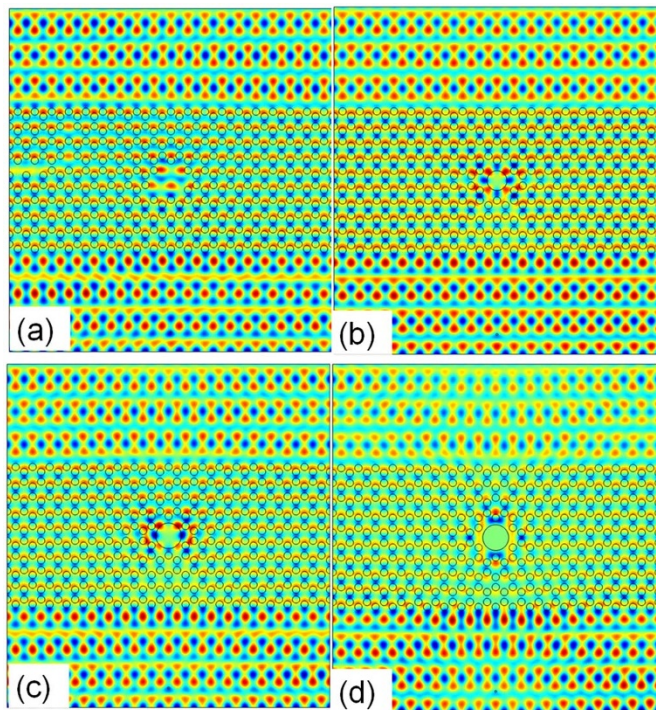
Figure 7 | **Plane wave transmission pattern with various kinds of defects.**
(a) Random distributed defects. A metallic cylindrical defect of (b) $r = 1$ m
and (c) $r = 1.3$ m. (d) An air bubble defect ($r = 1.3$ m). All of them show a
Talbot effects regardless of the type of defects.

in triangular lattice, the propagation of wave in our PC at Dirac cone
frequency is more insensitive to defects. At the frequency of ω_2, the
defect cannot be detected from the transmitted pattern, while it can
be easily found at the frequencies of ω_1 and ω_3. According to the field
distributions shown in Fig. 5(a2) and 5(c2), more than one mode are
excited in the PC at the frequencies of ω_1 and ω_3. These modes are all
attributed by the scattering of the defect, which would provide vari-
ous scattering wave vectors. As the EFC shown in Figs. 3(b1) and
3(b2), it is a circle near the frequency ω_0 compared to two big hexa-
gons at the frequencies of ω_1 and ω_3. Considering the incident angle
dependence, one wave vector of incident waves would often excite
two outgoing modes near ω_0, however, such two outgoing modes
would share the same Bloch wave vector due to the double degen-
eracies [shown in Fig. 1]. Furthermore, the existence of defect con-
tributes to wave vectors with various directions. Thus, we can
conclude that these two states near ω_0 are insensitive to incidence
direction of wave vectors[29]. But, at the frequencies of ω_1 and ω_3, two
non-degenerated modes are excited corresponding to two different
Bloch wave vectors, which are dependent on the incidence angle.

To check the angle dependent propagation properties in our sys-
tem, we employ a cylindrical incidence source which can provide
various wave vectors [shown in Fig. 6]. Similar to the case with the
plane-wave incidence source, Fig. 6(b1) also shows a Talbot effect.
The defects in this system cannot be detected at the frequencies near
ω_0 [shown in Fig. 6(b2)], which can be regarded as a type of cloak-
ing[11,12]. The negative refraction also can be realized in Fig. 6(a1)[30,31].

Moreover, the Talbot effect is immune to various types of defects
instead of special cases. Figure 7(a) shows the case of a random
distribution with several defects, and the transmission pattern is
similar to Fig. 5(b1). With metallic defects ($\rho_2 = 7670$ kg/m^3, $c_2 =$
6010 m/s, $r = 1$ m in Fig. 7(b) and $r = 1.3$ m in Fig. 7(c)), the
scattering of the cylinder is well suppressed. To further demonstrate
the ability to reduce the scattering cross section, we introduce an air
bubble ($r = 1.3$ m) which has a strong scattering field in usual

underwater acoustic system shown in Fig. 7(d). The scattering of
the air bubble is also effectively suppressed.

Discussion
In summary, we have designed a two-dimensional phononic hon-
eycomb lattice to achieve a quadruple-degenerate state at Γ point
which is constructed by the accidental degeneracy of two double-
degenerate states. In the vicinity of the quadruple-degenerate state,
there exist double isotropic linear Dirac cones. The linear dispersion
induced by the accidental degeneracy is rigorously analyzed by the
group representation theory. By using the $\vec{k}\cdot\vec{p}$ method, a 4×4
reduced Hamiltonian is obtained to describe the massless Dirac lin-
ear dispersion relation. The Berry phase of such double Dirac cones
cancels out due to the absence of the imaginary part. Although there
is no flat band in our system, and it neither satisfies long wave
approximation nor is regarded as effective zero-index medium, a
new kind of novel Talbot effect can still be found in this phononic
crystal near the quadruple degenerate point due to the linear and
isotropic dispersion, which is insensitive to various types of defects
and wave source. The *Zitterbewegung* is also expected for such quad-
ruple-degenerate state associated with the Dirac equation[32,33]. The
enhancement of the nonlinearity is also prospective for the phase
matching effect in our system[34,35].

Methods
Throughout the paper, the Finite Element Method (FEM) based on commercial
software COMSOL Multiphysics is employed for the numerical computations and the
simulations. The materials applied in simulations are water and steel. Plane wave
radiation boundary conditions are set on the outer boundaries of simulation domain
so there will be no interference from the reflected acoustic wave and the periodic
boundary condition are employed in the left and right boundaries to simulate the PC
with infinite size. The largest mesh element size is set lower than 1/20 of the shortest
wavelength.

1. Zhang, Y. B., Tan, Y. W., Stormer, H. L. & Kim, P. Experimental observation of the
    quantum Hall effect and Berry's phase in graphene. *Nature* **438**, 201–204 (2005).
2. Katsnelson, M. I. Zitterbewegung, chirality, and minimal conductivity in
    graphene. *Eur. Phys. J. B* **51**, 157–160 (2006).
3. Katsnelson, M. I., Novoselov, K. S. & Geim, A. K. Chiral tunnelling and the Klein
    paradox in graphene. *Nature Phys.* **2**, 620–625 (2006).
4. Sepkhanov, R. A., Bazaliy, Y. B. & Beenakker, C. W. J. Extremal transmission at the
    Dirac point of a photonic band structure. *Phys. Rev. A* **75**, 063813 (2007).
5. Castro Neto, A. H., Guinea, F., Peres, N. M. R., Novoselov, K. S. & Geim, A. K. The
    electronic properties of graphene. *Rev. Mod. Phys.* **81**, 109–162 (2009).
6. Torrent, D. & Sánchez-Dehesa, J. Acoustic analogue of graphene: observation of
    Dirac cones in acoustic surface waves. *Phys. Rev. Lett.* **108**, 174301 (2012).
7. Plihal, M. & Maradudin, A. A. Photonic band structure of two-dimensional
    systems: The triangular lattice. *Phys. Rev. B* **44**, 8565–8571 (1991).
8. Ochiai, T. & Onoda, M. Photonic analog of graphene model and its extension:
    Dirac cone, symmetry, and edge states. *Phys. Rev. B* **80**, 155103 (2009).
9. Han, D., Lai, Y., Zi, J., Zhang, Z.-Q. & Chan, C. T. Dirac Spectra and Edge States in
    Honeycomb Plasmonic Lattices. *Phys. Rev. Lett.* **102**, 123904 (2009).
10. Bittner, S. *et al.* Observation of a Dirac point in microwave experiments with a
    photonic crystal modeling graphene. *Phys. Rev. B* **82**, 014301 (2010).
11. Huang, X., Lai, Y., Hang, Z. H., Zheng, H. & Chan, C. T. Dirac cones induced by
    accidental degeneracy in photonic crystals and zero-refractive-index materials.
    Nature Mater. **10**, 582–586 (2011).
12. Liu, F., Huang, X. & Chan, C. T. Dirac cones at k = 0 in acoustic crystals and zero
    refractive index acoustic materials. *Appl. Phys. Lett.* **100**, 071911 (2012).
13. Liu, F., Lai, Y., Huang, X. & Chan, C. T. Dirac cones at k = 0 in phononic crystals.
    Phys. Rev. B **84** 224113 (2011).
14. Moitra, P., Yang, Y., Anderson, Z., Kravchenko, I. I. & Valentine4, D. P. B. J.
    Realization of an all-dielectric zero-index optical metamaterial. *Nature Photon.* **7**,
    791–795 (2013).
15. Wu, Y., Li, J., Zhang, Z.-Q. & Chan, C. T. Effective medium theory for
    magnetodielectric composites: Beyond the long-wavelength limit. *Phys. Rev. B* **74**
    085111 (2006).
16. Zhu, X., Liang, B., Kan, W., Zou, X. & Cheng, J. Acoustic cloaking by a superlens
    with single-negative materials. *Phys. Rev. Lett.* **106**, 014301 (2011).
17. Zhang, S., Xia, C. & Fang, N. Broadband acoustic cloak for ultrasound waves. *Phys.
    Rev. Lett.* **106**, 024301 (2011).
18. Sakoda, K. & Zhou, H. Analytical study of two-dimensional degenerate
    metamaterial antennas. *Opt. Express* **19**, 13899–13921 (2011).
19. John, D., Joannopoulos, S. G. J., Joshua N. Winn. & Robert, D. Meade. *Photonic
    Crystals: Molding the Flow of Light* (Princeton University Press, New Jersey, 2008).

20. Mei, J., Wu, Y., Chan, C. T. & Zhang, Z. Q. First-principles study of Dirac and Dirac-like cones in phononic and photonic crystals. *Phys. Rev. B* **86**, 035141 (2012).
21. Sakoda, K. Double Dirac cones in triangular-lattice metamaterials. *Opt. Express* **20**, 9925–9939 (2012).
22. Kafesaki, M. & Economou, E. N. Multiple-scattering theory for three-dimensional periodic acoustic composites. *Phys. Rev. B* **60**, 11993–12001 (1999).
23. Li, J. & Chan, C. T. Double-negative acoustic metamaterial. *Phys. Rev. E* **70**, 055602 (2004).
24. Li, Y., Wu, Y., Chen, X. & Mei, J. Selection rule for Dirac-like points in two-dimensional dielectric photonic crystals. *Opt. Express* **21**, 7699–7711 (2013).
25. M, S. Dresselhaus, G. D. & A. Jorio. *Group Theory: Application to the Physics of Condensed Matter* (Springer-Verlag, Berlin, Heidelberg, 2008).
26. Bolte, J. & Keppeler, S. A semiclassical approach to the dirac equation. *Ann. Phys.* **274**, 125–162 (1999).
27. Leger, J. R. & Swanson, G. J. Efficient array illuminator using binary-optics phase plates at fractional-Talbot planes. *Opt. Lett.* **15**, 288–290 (1990).
28. Talbot, H. F. Facts relating to optical science. *No. IV, Philos. Mag.* **9** (1836).
29. Cheng, Q., Jiang, W. X. & Cui, T. J. Spatial power combination for omnidirectional radiation via anisotropic metamaterials. *Phys. Rev. Lett.* **108**, 213903 (2012).
30. Lu, M.-H. *et al.* Negative birefraction of acoustic waves in a sonic crystal. *Nature Mater.* **6**, 744–748 (2007).
31. Christensen, J. & Javier Garcia de Abajo, F. Anisotropic metamaterials for full control of acoustic waves. *Phys. Rev. Lett.* **108**, 124301 (2012).
32. Zhang, X. Observing zitterbewegung for photons near the dirac point of a two-dimensional photonic crystal. *Phys. Rev. Lett.* **100**, 113903 (2008).
33. Zhang, X. & Liu, Z. Extremal transmission and beating effect of acoustic waves in two-dimensional sonic crystals. *Phys. Rev. Lett.* **101**, 264303 (2008).
34. Krutyanskiy, V. *et al.* Plasmonic enhancement of nonlinear magneto-optical response in nickel nanorod metamaterials. *Phys. Rev. B* **87**, 035116 (2013).
35. Suchowski, H. *et al.* Phase mismatch-free nonlinear propagation in optical zero-index materials. *Science* **342**, 1223–1226 (2013).

Author contributions

Z.G.C. carried out the numerical simulations and theoretical analysis. X.N., X.C.S. and L.Y.Z. contributed in the discussion of theoretical analysis. M.H.L. and Y.F.C. conceived and supervised the study. Z.G.C., Y.W., C.H. and M.H.L. wrote the paper.

Additional information

Competing financial interests: The authors declare no competing financial interests.

How to cite this article: Chen, Z.-G. *et al.* Accidental degeneracy of double Dirac cones in a phononic crystal. *Sci. Rep.* **4**, 4613; DOI:s10.1038/srep04613 (2014).